ECS Sensors Plus

Electrochemical Detection of H_2O_2 Using an Activated Glassy Carbon Electrode

ECS Sensors Plus, 2022 **1** 034401

Electrochemical Detection of H_2O_2 Using an Activated Glassy Carbon Electrode

Preethika Murugan,[1,2,=] Ramila D. Nagarajan,[3,=] Ashok K. Sundramoorthy,[1,*,z] Dhanraj Ganapathy,[1] Raji Atchudan,[4,=] Deepak Nallaswamy,[1] and Ajit Khosla[5,6,*]

[1]*Centre for Nano-Biosensors, Department of Prosthodontics, Saveetha Dental College and Hospitals, Saveetha Institute of Medical and Technical Sciences, Velappanchavadi, Chennai, 600077, Tamil Nadu, India*
[2]*Department of Chemistry, SRM Institute of Science and Technology, Kattankulathur 603203, India*
[3]*Department of Chemistry, V. V. Vanniaperumal College for Women, Virudhunagar-626001, Tamil Nadu, India*
[4]*School of Chemical Engineering, Yeungnam University, Gyeongsan 38541, Republic of Korea*
[5]*Department of Mechanical System Engineering, Graduate School of Science and Engineering, Yamagata University, Yonezawa, Yamagata, 992-8510, Japan*
[6]*Department of Applied Chemistry, School of Advanced Materials and Nanotechnology, Xidian University, Xi'an 710126, People's Republic of China*

Hydrogen peroxide (H_2O_2) is extensively used for sterilization purposes in the food industries and pharmaceuticals as an antimicrobial agent. According to the Food and Agriculture Organization (FAO), the permissible level of H_2O_2 in milk is in the range of 0.04 to 0.05% w/v, so it has been prohibited to use as a preservative agent. Herein, we reported the electrochemical sensing of H_2O_2 in milk samples using an activated glassy carbon electrode (AGCE). For this purpose, activation of GCE was carried out in 0.1 M H_2SO_4 by continuous potential sweeping between −0.7 to 1.8 V for 25 cycles. The AGCE showed a redox peak at -0.18 V in the neutral medium corresponding to the quinone functional groups present on the electrode surface. AGCE was studied in (pH 7.4) 0.1 M PBS for the electro-catalysis of H_2O_2. The surface of the activated electrode was analysed by Raman spectroscopy and contact angle measurements. In addition, for the activated surface, the contact angle was found to be 85° which indicated the hydrophilic nature of the surface. The different optimization parameters such as (1) effect of electrolyte ions, (2) electrooxidation cycles, and (3) oxidation potential windows were studied to improve the activation process. Finally, AGCE was used to detect H_2O_2 from 0.1 to 10 mM and the limit of detection (LOD) was found to be 0.053 mM with a linear correlation coefficient (R^2) of 0.9633. The selectivity of the sensor towards H_2O_2 was carried out in the presence of other interferents. The sensitivity of the AGCE sensor was calculated as 17.16 μA mol cm^{-2}. Finally, the commercial application of the sensor was verified by testing it in milk samples with H_2O_2 in the recovery range of 95%–98%.

 [DOI: 10.1149/2754-2726/ac7c78]

Manuscript submitted April 13, 2022; revised manuscript received June 27, 2022. Published July 14, 2022.

Hydrogen peroxide (H_2O_2) is a well-known effective bactericidal and sporicidal agent.[1,2] In the food, pharmaceutical and medical industries, liquid and vapour phases of H_2O_2 were commonly used to eliminate bacterial contaminants.[3,4] It is also used for controlling microbial deterioration of relevant products in the food industries.[5] Apart from various applications, H_2O_2 is one of the major adulterants found in milk that has been commonly reported in the developing countries.[6–8] The practice of using H_2O_2 is to activate the essential lactoperoxidase enzyme system which improves the quality of raw dairy products in the region where cooling is not extensively available.[9] The Food and Drug Administration (FDA) of the USA has permitted to use of H_2O_2 in the production of cheese.[10] Due to the chemical process that takes place inside the milk, it can contain only 1–2 mg l^{-1} of H_2O_2, this concentration range must be ten times high to terminate the pathogens.[11] If the concentration of H_2O_2 increases which in turn leads to negative consequences on the consumers.[12,13] The high concentration of H_2O_2 in the human system may lead to the degradation of various nutritional compounds which is vital for the physiological role.[14] The common beverages such as tea and coffee contain 100 μM of H_2O_2.[15] Therefore, it is more important to track the concentration of H_2O_2 in important food samples. Apart from the above examples, H_2O_2 is also formed due to knock-on effect in various enzyme catalysed reactions such as glucose, lactate and cholesterol oxidase reactions.[16] As a result, the increased level of H_2O_2 may lead to carcinogenesis and cardiac arrest in humans.[17] For a healthy person, the H_2O_2 concentration should be $<$10 nM in blood and plasma, however, it may increase in the plasma samples collected from the unhealthy persons (from 1–5 μM).[18] Until now many researchers have attempted to detect the H_2O_2 through various methods such as electrochemical,[19–21] chromatography,[7] colorimetric,[22,23] luminescent,[24] and spectrophotometric methods.[25,26]

Over the past decades, diverse types of carbon-based electrodes have been developed with various scopes and sensitivity for electroanalytical detection of important analytes.[27–31] The electron transfer rate can be enhanced by the pretreatment of carbon-based electrodes to observe an outstanding effect in the electrochemical activity.[32] Activation of the working electrodes has been carried out by various routes: (i) sweeping to a high positive potential, (ii) holding the electrode at a constant potential for a short period of time,[33–35] (iii) applying heat treatment,[36] (iv) ultrasonic polishing,[37] (v) oxygen plasma treatment,[38] (vi) mechanical activation,[39,40] etc. Thereby, electroanalytical properties have been improved after the electrode was activated which was ascribed to the attribution of surface functional groups and hydrophilicity.[41,42] As of now, many nanostructured carbon materials namely carbon nanotube (CNT), mesoporous carbon and graphene were used as the heterogeneous catalyst or catalyst support to improve the catalytic efficiency of the electrochemical reaction.[43] At a point of thriving interest, the carbon materials by themselves may act as an electrocatalyst during the reaction. Considering all the factors of carbon as the electrode material, we have decided to use the glassy carbon (GC), a non-graphitic carbon form, which was obtained by the pyrolysis of certain polymeric precursors. GC structure consists of discrete fragments of curved carbon planes which resembled imperfect fullerene. GC was synthesized at the temperature above 2000 °C which showed a network of stacked graphite with the random and tangled structure of carbon planes of dense structure.[44]

The oxidation of carbon material might occur at high anodic potential that would give rise to the deterioration of the electrode surface and also the electrochemical performance of the catalyst may

[=]Equal Contributions.
[*]Electrochemical Society Member.
[z]E-mail: ashok.sundramoorthy@gmail.com

get affected in terms of oxidation or reduction potential shift.[44–46] In some cases, the electrochemical oxidation of carbon could be beneficial for electrochemical sensors because oxidized surface may lead to faster electron transfer kinetics.[47] Generally, the electrochemical activity of the materials can be improved by incorporating the active functional groups via. thermal, chemical or electrochemical treatment. For examples, CNTs synthesized with the defects on their sidewalls or on the both end of the tubes were considered as edge plane-like defects, which promoted the electrocatalytic activity of CNTs towards various bio-molecules/chemicals.[28] Prasad et al. reported that introduction of edge plane carbonyl groups on the screen-printed electrode that enhanced the electron transfer rate of NADH oxidation.[48] Understanding the benefits of oxygen functionalities and edge plane-like sites on the activated GCE (AGCE), they found to be beneficial for various applications. The carbon-based electrodes could enhance the electron transfer rate of an analyte's oxidation or reduction process after the pre-treatment due to various factors (increased hydrophilicity, oxygen containing functional groups, surface roughness, etc).[49] Generally, the electrochemical activation process may generate some functional groups like hydroxyl, carboxyl, and quinone on the surface of the GCE. These functional groups could act as electron transfer mediators in a reaction that can improve the sensitivity and selectivity of the sensors.

In this study, we have reported the electrocatalytic reduction of H_2O_2 on an activated GCE in PBS. Firstly, GCE was oxidized in 0.1 M H_2SO_4 which resulted in quinone like redox peak on the GCE that was used for the electro-reduction of H_2O_2 at a reduced overpotential of −0.4 V with enhanced peak current (Scheme 1). The activated electrode's surface was analysed by Raman spectroscopy and contact-angle measurements. Secondly, we have optimized the various parameters such as selection of electrolytes, number of electrooxidation cycles, and oxidation potential windows to achieve the best performance against H_2O_2. As-prepared AGCE showed a linear response for H_2O_2 in the range from 0.1–10 mM with high selectivity compared to other interfering compounds. Finally, the application of the AGCE was demonstrated by sensing of H_2O_2 in milk samples with good recovery percentages.

Experimental

Materials and characterizations.—Sulphuric acid (H_2SO_4), sodium hydroxide (NaOH), hydrogen peroxide (H_2O_2) (30%), sodium dihydrogen phosphate monohydrate ($H_2NaPO_4.H_2O$), and sodium phosphate dibasic heptahydrate ($Na_2HPO_4.7H_2O$) were purchased from Sigma-Aldrich, India. Ascorbic acid (AA), Oxalic acid (OA), Dopamine (DA) and Uric acid (UA) were purchased from SRL, India. All the chemicals were used without further purifications. Distilled water (18.2 MΩ cm@ 25 ± 2 °C) was obtained from a Millipore ultrapure water system. Raman spectra were recorded using the 633 nm laser at an average of 5 spots (LabRAM HR evolution, Horiba) connected to an Olympus imaging microscope (Labspec6 Raman software). The contact-angle was measured using Drop master (DMs-401), Kyowa Interface Science Co., Ltd. Electrochemical studies were performed by using an electrochemical workstation (CHI-760E, CH Instrument, USA). A conventional three-electrode system was employed with the Ag/AgCl (3 M KCl) and platinum wire as a reference and counter electrodes.

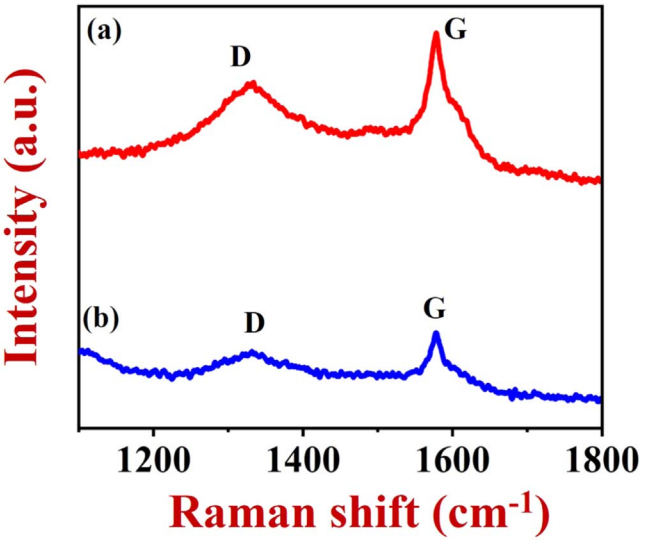

Figure 1. Raman spectra were recorded for (a) ASPE and (b) SPE using the wavelength of 633 nm laser.

Pre-treatment of bare GCE.—Initially, a bare GCE (3 mm ϕ) was polished with a series of 1 μm, 0.3 μm and 0.05 μm alumina slurries on a cleaning pad to achieve a mirror-like surface. After that, GCE was sonicated in deionized water and ethanol for a few minutes. Finally, GCE was rinsed with deionized water and dried.

Electrochemical activation of GCE.—The electro-activation of GCE or SPE (screen-printed carbon electrode received from CH Instruments, USA) was carried out in 0.1 M H_2SO_4.[44,49] The activation process was carried out by sweeping the working electrode (GCE) in the potential range between −0.7 and 1.8 V for 25 cycles at a scan rate of 50 mV/s. During this oxidation process, various functional groups (carbonyl, carboxyl, quinone, etc.) were generated on the surface of GCE. As-prepared AGCE exhibited a redox peak at −0.1 V[50] with a high peak current of 2 μA due to the surface bounded redox functional groups (hydroquinone). Compared to bare GCE, AGCE showed a current efficiency higher than 20%, which involved in the electroreduction process of H_2O_2.

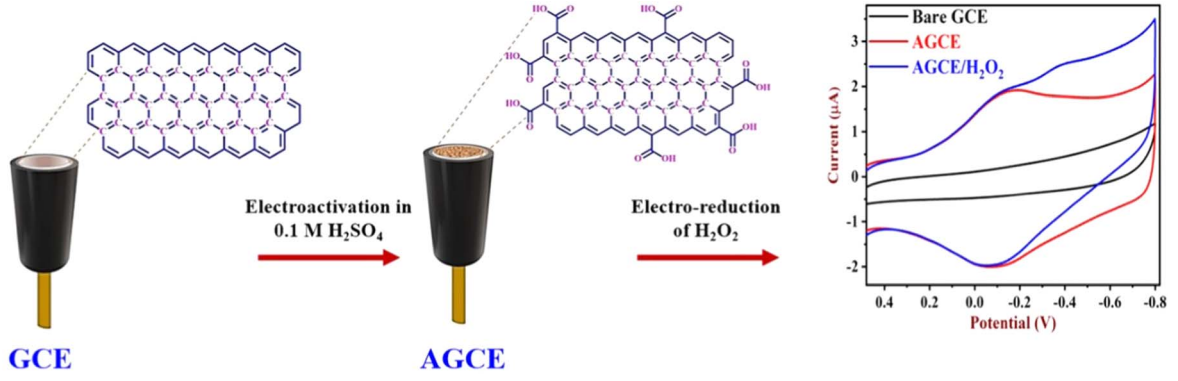

Scheme 1. Schematic representation of AGCE activation process for the electro-catalytic reduction of H_2O_2.

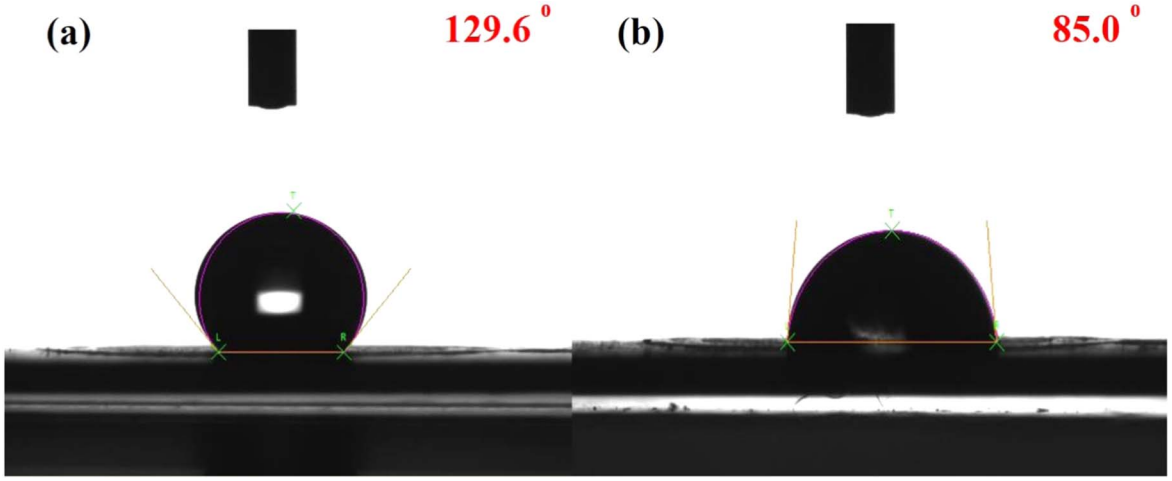

Figure 2. Contact angle measurements were made on the (a) SPE and (b) ASPE substrates.

Results and Discussion

Raman spectroscopy.—The Raman spectra were recorded for the bare SPE and ASPE (electro-activated screen-printed carbon electrode) with the excitation wavelength of 633 nm. Both the unmodified SPE and ASPE showed the major "D" (at 1369 cm^{-1}) and "G" bands (at 1572 cm^{-1}) corresponded to the structural deformation on the sp^2 carbon network and also due to the plane stretching motion of sp^2 carbon atoms (Figs. 1a–1b).[51] Compared to untreated SPE (curve b), ASPE showed a higher disorder "D" band and enhanced "G" band which indicated a high degree of surface oxidation and functionalization (Fig. 1, curve a). The rate of electro-oxidation and defects created on the electrode surface was analysed by the I_D/I_G ratio.[52,53] The I_D/I_G ratio for the bare SPE was 0.83. In the case of ASPE, due to higher disorder and defects on the surface, the I_D/I_G ratio was increased to 1.01 (Fig. 1, curve a). It further indicated the presence of more defects on the ASPE[54,55] as confirmed by Raman spectra. It was expected that the activated electrode could help in the electrochemical reduction of H_2O_2 compared to the bare SPE.[56]

Contact angle measurements.—The wetting properties of the solid electrode surface by a liquid can be done using the contact angle measurement. When the contact angle value is less than 90°, then it is known as a hydrophilic surface. If it is more than 90°, then it is called as a hydrophobic surface.[57] The wettability nature of the surface was studied for bare SPE as shown in Fig. 2a, where the contact angle of the bare SPE was 126°. This showed that the bare SPE surface was hydrophobic in nature before electro-oxidation. However, for ASPE, the contact angle was found to be 85° which clearly indicated the hydrophilic surface was formed by the electro-activation process (Fig. 2b). This process was also resulted in the generation of hydroxyl, carboxyl and quinone groups on the electrode surface.[56]

Electro-reduction of H_2O_2 on AGCE.—To ascertain the electrocatalytic activity of the AGCE against H_2O_2, cyclic voltammograms (CVs) were recorded in (N_2 saturated) 0.1 M PBS using both bare GCE and AGCE. When the potential was scanned between 0.5 and −0.8 V, the bare GCE showed only the non-faradaic current response. Even after the addition of 1 mM H_2O_2, bare GCE did not exhibit a reduction peak current of H_2O_2 (Fig. 3, curves i and ii). Interestingly, when the AGCE was cycled in the same potential window, a new redox peak was appeared. During the electro-activation process, the quinone-like groups were formed on the GCE surface which exhibited the redox peak at −0.18 V in 0.1 M PBS. Next, the AGCE was scanned in the same potential window with 1 mM H_2O_2 in 0.1 M PBS. It was noted that the electro-reduction peak of H_2O_2 appeared at −0.4 V with a high cathodic

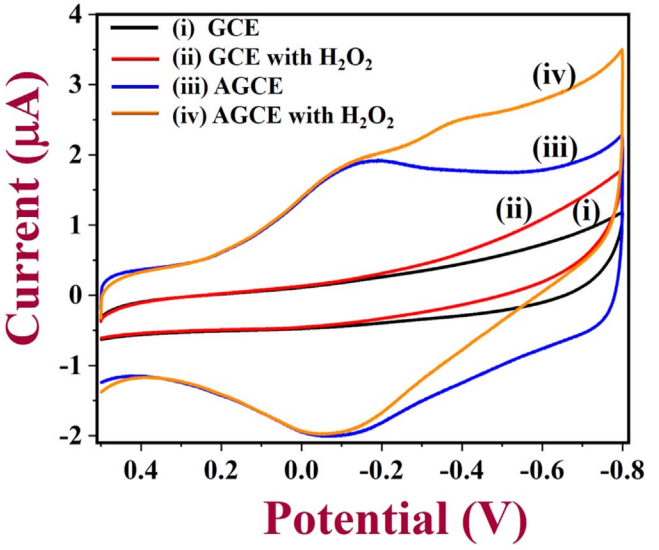

Figure 3. CVs were recorded using bare GCE in 0.1 M PBS (pH 7.4) in the absence (curve i) and presence of 1 mM H_2O_2 (curve ii). CVs were recorded using AGCE in 0.1 M PBS (pH 7.4) in the absence (iii) and presence of 1 mM H_2O_2 (iv). Scan rate = 50 mV s^{-1}.

peak current (2.5 μA) (Fig. 3, curves iii and iv). From this observation, we found that AGCE had high catalytic activity against H_2O_2 than the bare GCE. This enhanced electro-catalytic activity of AGCE can be credited to the surface covered quinone-like functional groups which acted as the electron transfer mediator for the reduction of H_2O_2 (**Scheme 2**). The functional groups of the AGCE might have transferred the electrons to H_2O_2 and reduced the overpotential of H_2O_2 reduction. This electro-activation process was simple and easy to do in a short period of time, so this method can be adopted for the electrochemical reduction of H_2O_2.

Effect of electrolytes on the activation process.—The role of electrolyte ions in the electro-activation process was studied using different electrolytes. For this purpose, GCE was separately oxidized in 0.1 M NaOH as given in the experimental section . Similarly, we have also employed other electrolytes such as acetate buffer, H_2SO_4 and PBS for electro-activation process. After that, every one of AGCE's was used to record CVs in 0.1 M PBS. As shown in Fig. 4A, all of them exhibited a redox peak at −0.18 V, which corresponded to the redox process of functional groups present on the GCE surface (quinones). We have also compared the reduction peak currents of each modified electrode. It was confirmed that GCE

Scheme 2. Schematic representation of AGCE for the electro-catalytic reduction of H_2O_2.

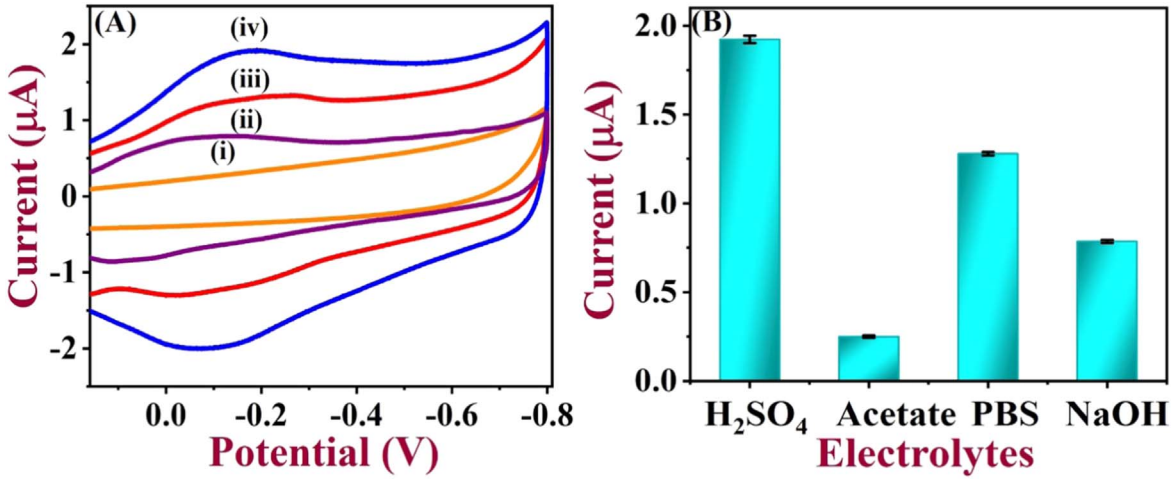

Figure 4. CVs were recorded using AGCE in 0.1 M PBS (pH 7.4) after it activated in different electrolytes at a scan rate of 50 mV s^{-1}. (i) acetate buffer, (ii) NaOH, (iii) PBS and (iv) H_2SO_4. (B) Bar diagram shows the peak currents of AGCE against the different electrolytes used for the activation.

activated in 0.1 M H_2SO_4 showed higher peak currents compared to other electrolytes (Fig. 4B). The mechanism of the activation process can be explained as given below:

The oxidized GCE showed a redox peak at the formal potential (E°′) of −0.18 V with high cathodic peak current of 1.8 μA. Due to the high dissociation of 0.1 M H_2SO_4, the H^+ and HSO_4^- ions attacked both cathode and anodes under the applied potential. The H^+ ion was reduced at the cathode meanwhile the SO_4^{2-} attacked the anode (GCE) and functionalized the electrode surface. It was the reason for the highest degree of oxidation occurred in the H_2SO_4 solution. Figure 4A also showed that the degree of oxidation was less on GCE when the acetate buffer was used which may be due to the poor dissociation of ions. After the sulphuric acid, the AGCE prepared in PBS showed high degree of oxidation with an activation current of 1.4 μA. Relatively, AGCE prepared in NaOH shifted the redox potential towards ∼0 V with a lower peak current. These data indicated that electrolyte ions might have played a major role in the activation process (Figs. 4A–4B). Finally, we have selected the H_2SO_4 for the GCE activation process.[58]

Optimization of activation potential window.—Next, the effect of the potential window on the activation process was also studied to achieve the best activated GCE. For this study, AGCE was prepared by potential sweeping in 0.1 M H_2SO_4 (between −0.7 and 1.0 V; −0.7 and 1.2 V; −0.7 and 1.5 V; and −0.7 and 1.8 V) at the scan rate of 50 mV s^{-1} for 25 cycles. After that CVs were recorded in 0.1 M PBS using all the AGCE's. As shown in the CVs (Fig. 5A), in the lower potential window (−0.1 to 1 V), the AGCE showed no redox peak. It indicated that electrode oxidation did not take place under the lower potential window's (curves i and ii) (Fig. 5B). The highest degree of activation was found under the applied potential of −0.1 to 1.8 V in 0.1 M H_2SO_4. The maximum oxidation peak current recorded was 1.9 μA (Fig. 5B). From these studies, it was concluded that potential window of −0.1 to 1.8 V was required to achieve higher activation on GCE in 0.1 M H_2SO_4. Under this high applied potential, anions effectively attacked the surface of GCE and created more functional groups.

Effect of potential cycles.—Furthermore, the number of CV cycles required for effective oxidation of GCE was also optimized in 0.1 M H_2SO_4. CVs were recorded using various AGCE's prepared by controlled activation in the applied potential window of −0.1 to 1.8 V by only varying the number of CV cycles as 10, 20, 25 and 30 cycles in 0.1 M H_2SO_4. As shown in Figs. 6A–6B, when the number of potential cycles were increased, the activation rate of GCE was also increased. The highest oxidation peak current (2.2 μA) was obtained for the AGCE prepared with 25 cycles. This study also indicated that beyond 25 CV cycles, activation of GCE reached a saturation point and peak currents started to decline for 30 cycles. We further selected 25 CV cycles for the activation of GCE in 0.1 M H_2SO_4.

Electrochemical characterization of AGCE and bare-GCE.—The CVs were recorded using both bare GCE and the AGCE in 0.1 M KCl containing 5 mM $[Fe(CN)_6]^{3-/4-}$. Both electrodes exhibited redox peaks corresponding to the $[Fe(CN)_6]^{3-/4-}$ with the peak-to-peak separation (ΔEp) of 100 mV and the formal potential (E°′) was 0.2 V. Interestingly, AGCE showed an enhanced oxidation peak current of about 32 μA which is higher than the bare GCE (26 μA), it confirmed that AGCE had high electrocatalytic activity (Fig. 7(A), curves i, ii). Next, AGCE was used to record CVs at different scan rates from 10 to 100 mV s^{-1}, it showed that peak currents were increased with the scan rate. The linear plot was prepared between the square root of scan rate and the reduction peak currents. The linear regression equation was $Y = -2.147 \times 10^{-3} + 2.513 \times 10^{-6}$ ($R^2 = 0.99$). The active surface area of the electrode was calculated using Randles-Sevcik equation (Eq. 1). The "n" is the number of electrons, D is the diffusion coefficient of $[Fe(CN)_6]^{3-/4-}$ (7.6×10^{-6} cm^2 s^{-1}), C_o is the concentration (5 mM), (ν) scan rate and A is the surface area of the electrode.

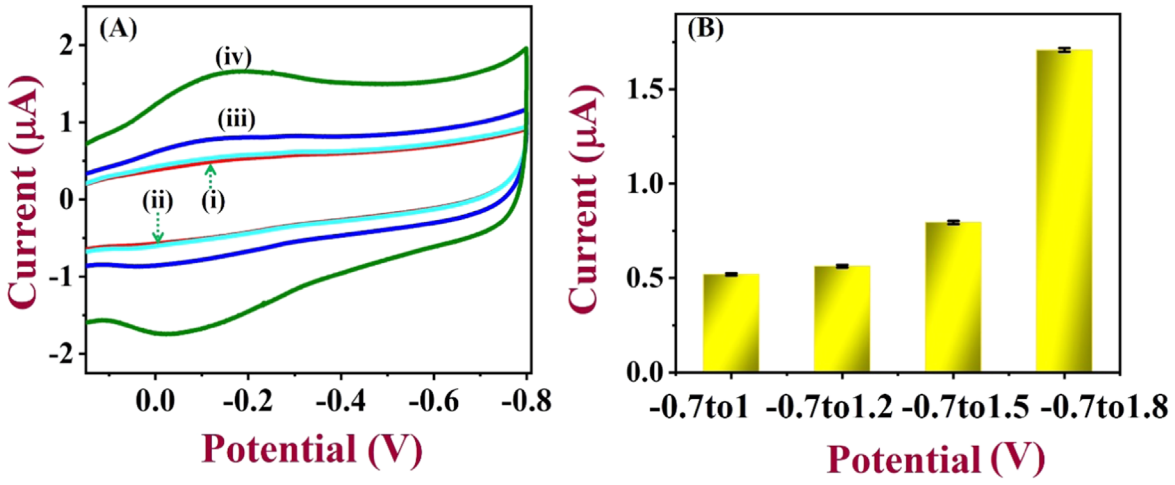

Figure 5. CVs were recorded in 0.1 M PBS (pH 7.4) at a scan rate of 50 mV s^{-1} using various AGCE's after it activated in 0.1 M H_2SO_4 by applying the different potential window: from (i) −0.7 to 1 V, (ii) −0.7 to 1.2 V, (iii) −0.7 to 1.5 V and (iv) −0.7 to 1.8 V. (B) Bar diagram was plotted between different potential windows used and reduction peak currents.

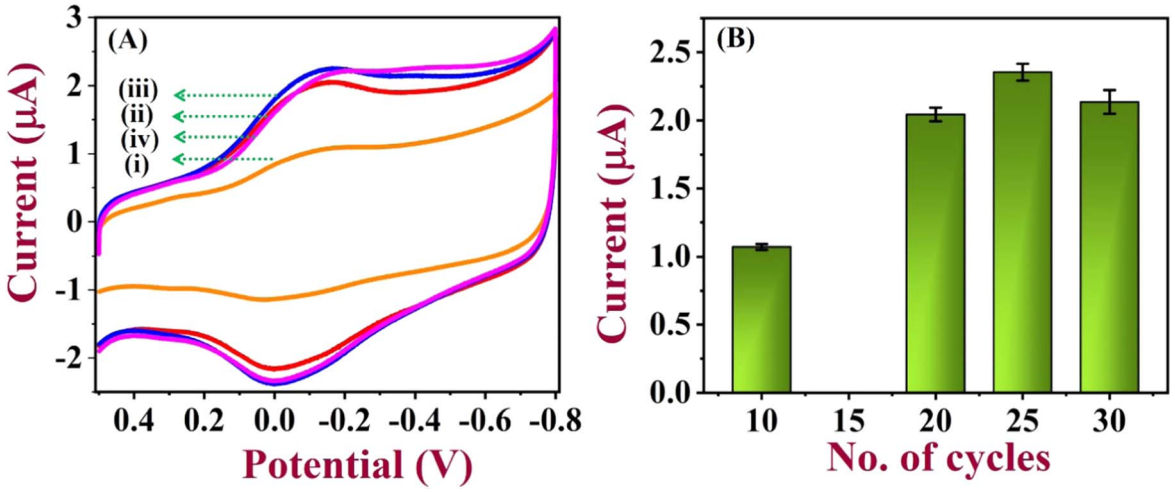

Figure 6. CVs were recorded using various AGCE's in 0.1 M PBS (pH 7.4) at a scan rate of 50 mV s^{-1}, after they have been activated with different potential cycles: (i) 10, (ii) 20, (iii) 25 and (iv) 30 cycles. (B) Bar diagram shows the effect of potential sweep cycles vs. peak currents.

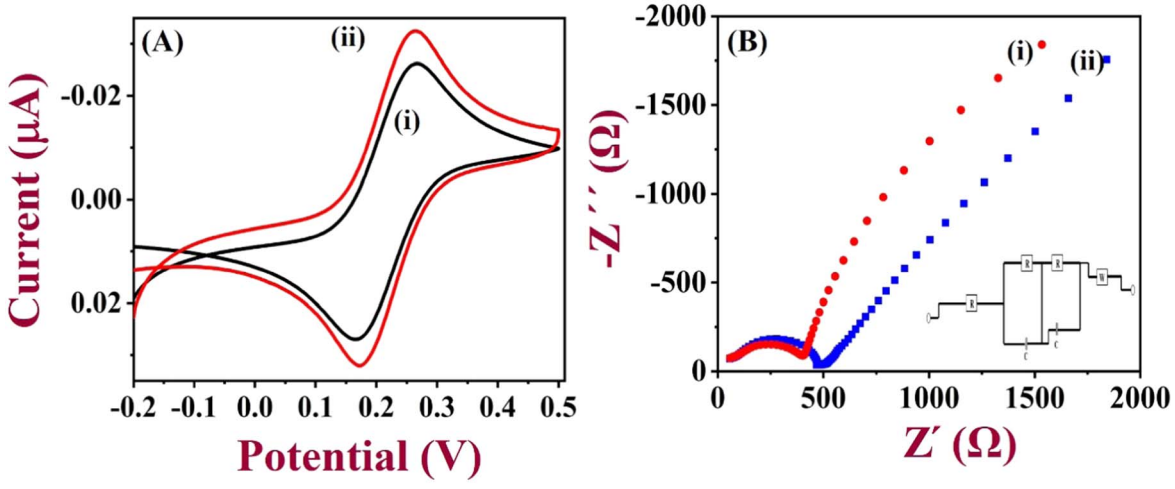

Figure 7. (A) CVs of (i) bare GCE (black) and (ii) AGCE (red) were recorded in 0.1 M KCl containing 5 mM $[Fe(CN)_6]^{3-/4-}$. (B) The Nyquist plots were recorded using (i) AGCE and (ii) bare GCE in 0.1 M KCl with 5 mM $[Fe(CN)_6]^{3-/4-}$ by applying an AC voltage with 5 mV amplitude.

$$I_{pa} = (2.69 \times 10^5) n^{3/2} D^{1/2} C_O \nu^{1/2} A \quad [1]$$

Using the above parameters, the "A" was calculated. The active surface areas of the bare GCE and AGCE's were found to be 0.11 and 0.58 cm^2. Compared to GCE, the AGCE showed more surface area. The conductivity of the electrode was also studied after electro-activation using electrochemical impedance spectroscopy (EIS). The Nyquist plots of bare-GCE and AGCE were recorded in 0.1 M KCl containing 5 mM $[Fe(CN)_6]^{3-/4-}$ by applying an AC voltage with 5 mV amplitude as shown in Fig. 7B. Both of the electrodes showed the Nyquist plots with the semicircle regions and the linear parts. This EIS data was also analyzed by fitting to an equivalent electrical circuit model as shown in Fig. 7B, inset. The solution resistance (R_s) and charge transfer resistance of the electrode (R_{ct}) were calculated. The R_s of the electrode were about 50 ohm and the semicircle portion indicated the R_{ct} of the electrode. The R_{ct} values for the bare GCE and the AGCE were found to be 450 and 350 Ω. This data also confirmed that AGCE had higher conductivity than the bare GCE, which may be used as an effective electrode for the reduction of H_2O_2.[59]

Effect of scan rate.—Figure 8A illustrates the CVs recorded using AGCE with different scan rates from 10 to 240 mV s^{-1} in 0.1 M PBS. When the scan rate increases, the redox peak currents corresponding to the AGCE were increased. At the same time, the peak potential was shifted a bit towards the higher positive potential. The linear plot was made between the scan rate and the redox peak currents of AGCE which showed the linear regression equation with the R^2values of 0.9972 and 0.9938 for the oxidation and the reduction peak currents, respectively (Fig. 8B). The effect of scan rate studies revealed that AGCE followed the surface-controlled process.[60]

Detection of H_2O_2 using AGCE.—Figure 9A showed the electrocatalytic activity of AGCE with the varying concentrations of H_2O_2 from 0.1 mM to 10 mM. The corresponding reduction peak currents were increased at the potential of −0.4 V upon the addition of various concentrations of H_2O_2 from 0.1 mM to 10 mM. However, after the addition of 10 mM concentration, the sensor had reached the saturation level. The limit of detection (LOD) was calculated using the formula of 3.3× standard deviation of the blank/slope of the calibration curve.[60] The obtained LOD was 0.053 mM (Fig. 9B) which was compared with the other modified electrodes as given in the table (Table I). The analytical sensitivity of the AGCE was calculated to be 17.16 μA mol cm^{-2}.

Selectivity of AGCE.—Selectivity of the electrochemical sensor is an important factor, so the selectivity of AGCE was tested with the other important interferent molecules such as AA, UA, glucose, lactose, etc. along with H_2O_2 (Fig. 10A).[30,60] The CVs were recorded using AGCE in the presence of 1 mM of H_2O_2 in 0.1 M PBS. Followed by, the same electrode was subjected to record CVs with the equal concentration (1 mM) of each interfering substance. As shown in Fig. 10A, AGCE responded selectively towards the reduction of H_2O_2 compared to other interferent molecules. The high selectivity of the sensor may be due to the unreactive nature of the interferent molecules under this reduction potential range. Next, the corresponding reduction peak currents were recorded after the addition of each interferent molecules. The bar diagram represented the changes in the reduction peak current of H_2O_2 after the addition of interferent molecules. As shown in Fig. 10B, the reduction peak current was decreased by about 8%, so we believe that this sensor may be more suitable for the selective detection of H_2O_2 (Fig. 10B).

Oxygen reduction reaction (ORR) at AGCE.—AGCE was also applied for the oxygen reduction reaction. CVs of the AGCE were recorded in the O_2 and N_2 saturated 0.1 M PBS. In the presence of dissolved oxygen in PBS, the AGCE showed a strong cathodic peak with high reduction current at −0.45 V (Fig. 11A, curve i). The same reaction was repeated in the N_2 saturated solution, but the corresponding O_2 peak current was not observed at −0.45 V (curve ii). These studies confirmed that AGCE had exhibited high electrocatalytic activity for the reduction of H_2O_2 as well as O_2. The AGCE also differentiated both the H_2O_2 and O_2 reduction peaks at different potentials of −0.4 and −0.45 V, respectively.[27] For comparison, O_2 reduction was carried out in 0.1 M PBS using the bare GCE, but the reduction of O_2 was observed at a higher negative potential (−0.7 V) with a lower peak current than the AGCE (Fig. 11B).

Stability study of AGCE.—The stability of the AGCE was studied by CVs. The CVs were recorded continuously using a AGCE for 50 cycles. The peak currents of the AGCE were maintained stable up to 90%, even after several measurements (Fig. 12). The data confirmed that as-prepared AGCE had exhibited good stability in the studied potential range.

Real sample analysis.—We tested extracts collected from milk samples after they were centrifuged at 15000 rpm. This step was used to remove the milk proteins/fats which may affect the sensor response.[65,66] To the electrolyte solution, the obtained supernatant portion of the milk sample was added and detection of H_2O_2 was performed before and after the standard additions of H_2O_2. The

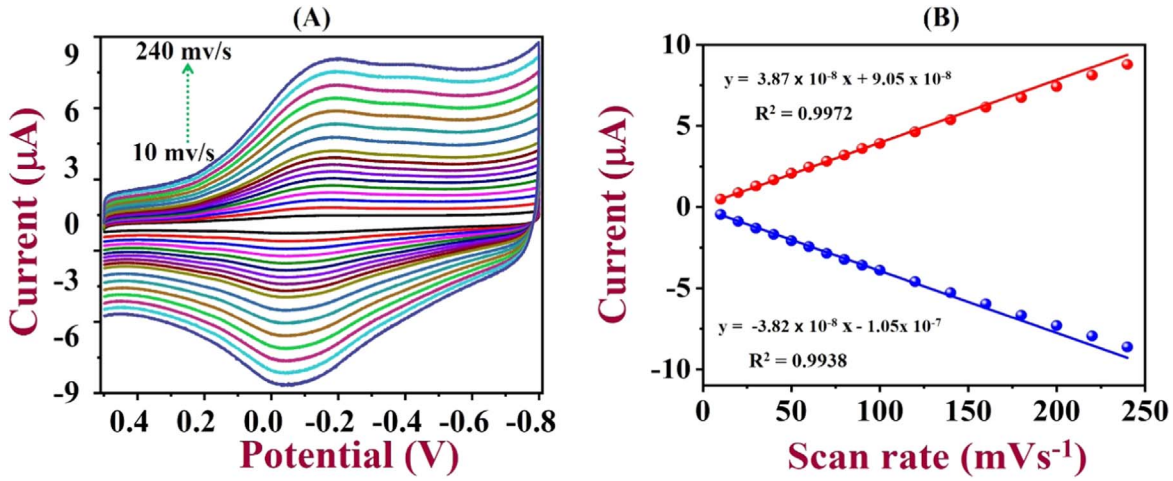

Figure 8. (A) CVs were recorded using an AGCE at different scan rates from 10 to 240 mV s^{-1} in 0.1 M PBS (pH 7.4). (B) A linear plot of redox peak currents of AGCE (I_{pa} and I_{pc}) vs. scan rates.

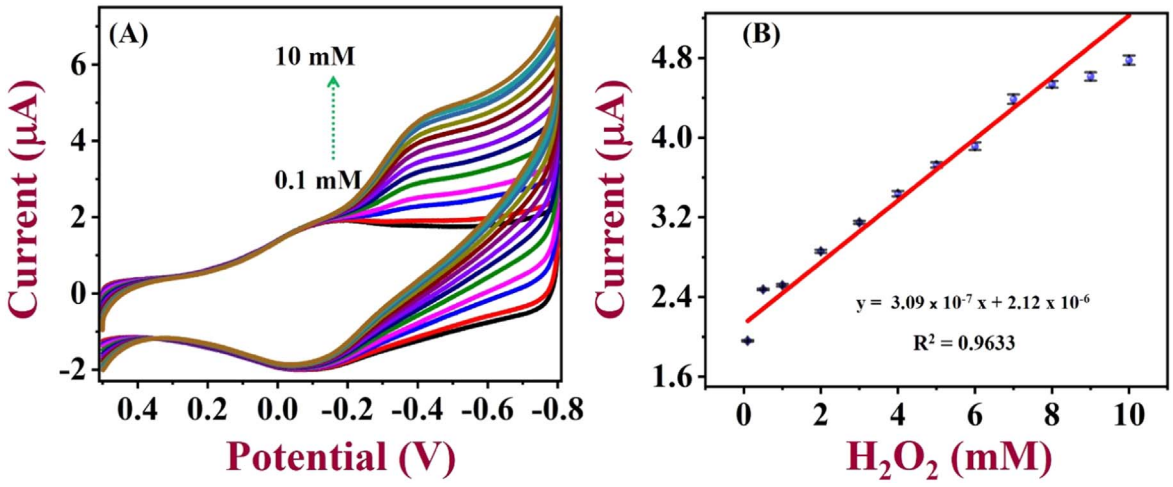

Figure 9. (A) CVs of AGCE were recorded in 0.1 M PBS (pH 7.4) containing different concentrations of H_2O_2 from 0.1 mM—10 mM at a scan rate of 50 mV s^{-1}. (B) A calibration graph was made between H_2O_2 reduction peak currents vs. [H_2O_2].

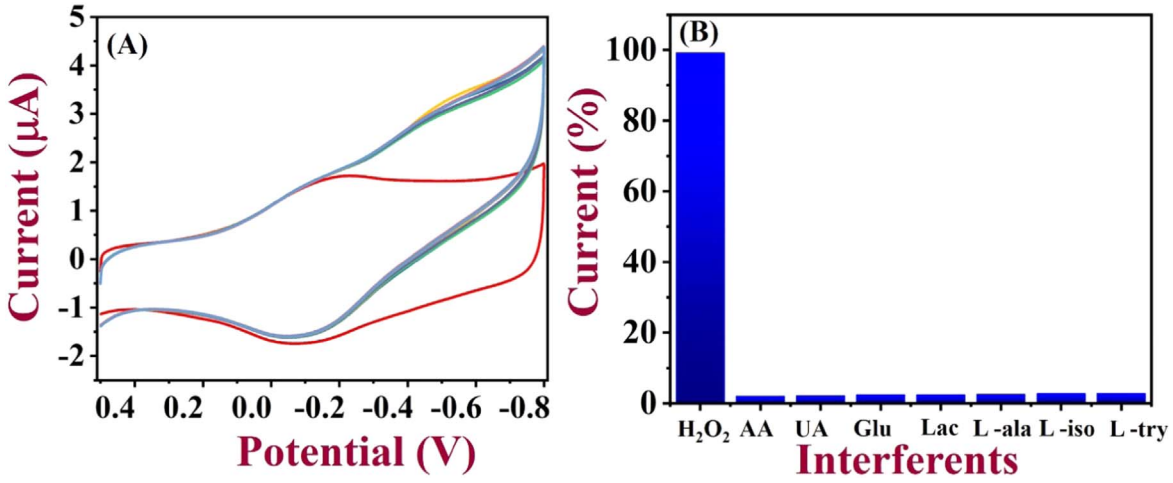

Figure 10. (A) CVs were recorded using a AGCE in 0.1 M PBS (pH 7.4) containing 1 mM H_2O_2 plus 1 mM of [AA, UA, glucose, lactose, L - alanine, L - isoleucine, and L - tyrosine]. (B) The bar diagram shows the changes in the reduction peak currents vs. interference molecules.

Table I. The comparison of the various reported electrochemical H_2O_2 sensors with the proposed method.

S. No.	Electrode Modification	Linear Range (mM)	LOD (mM)	References
1	HRP/chitosan–gelatin composite[a)]	0.1 to 1.7	0.05	61
2	PGG/graphene electrode[b)]	0.1–3.5	0.15	62
3	HRP–TiO_2/fCNT/GC[c)]	0.5–7.5	0.81	63
4	Pt nanoflower	0.1–0.9	0.06	64
5	AGCE	0.1–10	0.053	This work

a) HRP-Horse Radish Peroxidase. b) PGG-Peroxidase fromguinea grass. c) fCNT-Functionalised carbon Nanotube.

Table II. Detection of H_2O_2 in milk samples using AGCE as a sensor.

S. No.	Samples	Added (mM)	Found (mM)	Recovery (%)[a)]	RSD (%)
1	Milk	1	0.98	98	1.21
2	Milk	2	1.95	97.5	1.04
3	Milk	3	2.87	95.7	1.62

a) This experiment was repeated three times.

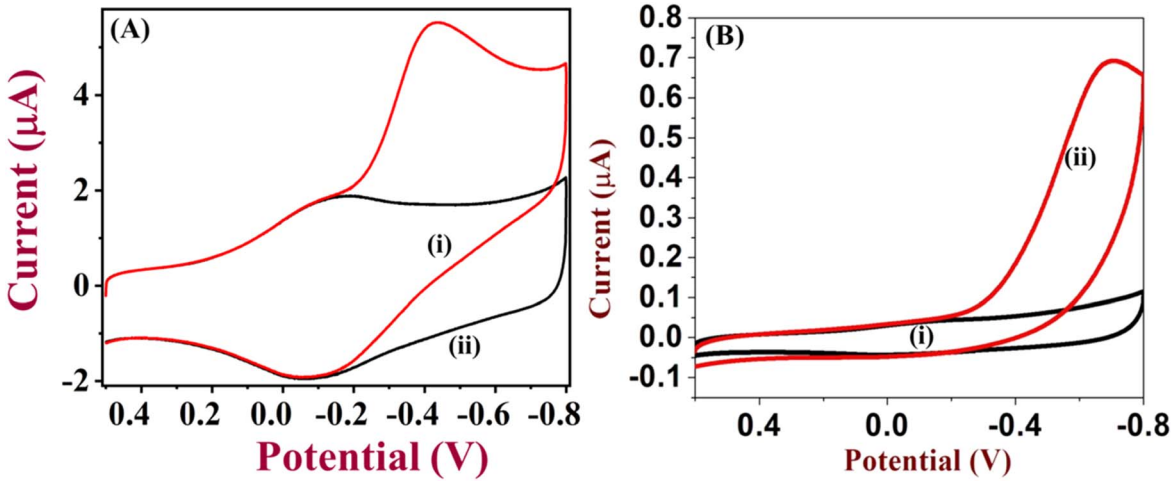

Figure 11. (A) CVs of AGCE were recorded in (i) O_2 saturated solution and (ii) N_2 saturated 0.1 M PBS (pH 7.4). (B) CVs of bare GCE were recorded in (i) N_2 saturated solution and (ii) O_2 saturated 0.1 M PBS (pH 7.4). Scan rate = 50 mV s^{-1}.

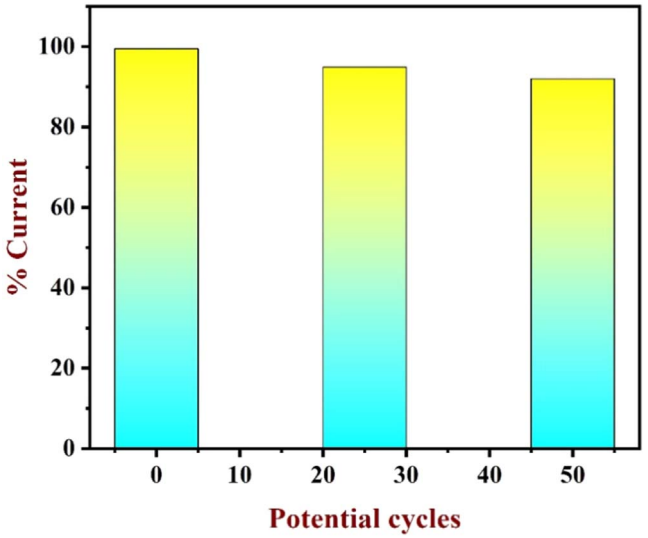

Figure 12. Stability study of AGCE was recorded by CVs in 0.1 M PBS up to 50 cycles at a scan rate of 50 mV s^{-1}.

recovery percentages were calculated using the formula of Recovery = $C_{found}/C_{Spiked} \times 100$ as shown in Table II.

4.Conclusions

In summary, for the first time, we have reported a simple method for the reduction of H_2O_2 in 0.1 M PBS using an AGCE. The GCE was oxidized in 0.1 M H_2SO_4 by continuous potential sweeping for 25 cycles. As-prepared AGCE was used as the sensor for the reduction of H_2O_2 at a reduced overpotential of −0.4 V with the high catalytic current. The different optimization studies were performed by varying the electrolyte, electrooxidation cycle, and oxidation potential window to achieve an effective activation process. Due to the high electrocatalytic activity, the AGCE showed a linear range of H_2O_2 detection from 0.1 to 10 mM with high selectivity towards H_2O_2 compared to other interferents. The real application of the sensor was also tested by detecting H_2O_2 in milk samples with a good recovery.

Acknowledgments

AKS thanks the Science and Engineering Research Board (SERB) for funding through CRG/2021/001517. We thank the Department of Science and Technology (DST) (International Bilateral Cooperation Division), India, for financial support through "INDO-RUSSIA Project (File No. INT/RUS/RFBR/385)."

ORCID

Ashok K. Sundramoorthy https://orcid.org/0000-0002-8512-9393
Ajit Khosla https://orcid.org/0000-0002-2803-8532

References

1. M. G. C. Baldry, *J. Appl. Bacteriol.*, **54**, 417 (1983).
2. M. A. Khadre and A. E. Yousef, *Int. J. Food Microbiol.*, **71**, 131 (2001).
3. V. N. Krukovsky, *J. Dairy Sci.*, **32**, 163 (1949).
4. N. H. Martin, A. Friedlander, A. Mok, D. Kent, M. Wiedmann, and K. J. Boor, *J. Food Prot.*, **77**, 1809 (2014).
5. M. Brennan, G. Le Port, and R. Gormley, *LWT-Food Sci. Technol.*, **33**, 285 (2000).
6. T. Azad and S. Ahmed, *Int. J. Food Contam.*, **3**, 22 (2016).
7. A. S. Ivanova, A. D. Merkuleva, S. V. Andreev, and K. A. Sakharov, *Food Chem.*, **283**, 431 (2019).
8. M. A. M. Salih and S. Yang, *J Adv Dairy Res*, **5**, 192 (2017).
9. E. Seifu, E. M. Buys, and E. F. Donkin, *Trends Food Sci. Technol.*, **16**, 137 (2005).
10. U. S. F. D. Administration, "Food and Drugs, 21 CFR 184.1366 - Hydrogen Peroxide." *Regulatory Information* (Code of Federal Regulations, FDA, USA) Annual edition ed., I April 1 (2011), https://www.govinfo.gov/app/details/CFR-2011-title21-vol3/CFR-2011-title21-vol3-sec184-1366/summary.
11. D. D. Muir, *Int. J. Dairy Technol.*, **49**, 24 (1996).
12. M. G. Dickens and K. J. Franz, *Chembiochem a Eur. J. Chem. Biol.*, **11**, 59 (2010).
13. M. E. Goetz and A. Luch, *Cancer Lett.*, **266**, 73 (2008).
14. R. A. B. Silva, R. H. O. Montes, E. M. Richter, and R. A. A. Munoz, *Food Chem.*, **133**, 200 (2012).
15. B. Halliwell, M. V. Clement, and L. H. Long, *FEBS Lett.*, **486**, 10 (2000).
16. M. Preethika and A. K. Sundramoorthy, *Appl. Surf. Sci.*, **488**, 503 (2019).
17. S. K. Maji, S. Sreejith, A. K. Mandal, X. Ma, and Y. Zhao, *ACS Appl. Mater. Interfaces*, **6**, 13648 (2014).
18. R. Gaikwad, P. R. Thangaraj, and A. K. Sen, *Sci Rep.*, **11**, 1 (2021).
19. J. Anojčić, V. Guzsvány, O. Vajdle, D. Madarász, A. Rónavári, Z. Kónya, and K. Kalcher, *Sensors Actuators B Chem.*, **233**, 83 (2016).
20. Z. Xu, L. Yang, and C. Xu, *Anal. Chem.*, **87**, 3438 (2015).
21. C. Zhang, L. Li, J. Ju, and W. Chen, *Electrochim. Acta*, **210**, 181 (2016).
22. M. E. Abbas, W. Luo, L. Zhu, J. Zou, and H. Tang, *Food Chem.*, **120**, 327 (2010).
23. S. S. Nanda, D. K. Yi, and K. Kim, *J. Nanosci. Nanotechnol.*, **16**, 1181 (2016).
24. Y. Li, X. You, and X. Shi, *Food Anal. Methods*, **10**, 626 (2017).
25. G. C. S. de Souza, P. A. B. da Silva, D. M. da, S. Leotério, A. P. S. Paim, and A. F. Lavorante, *Food Control*, **46**, 127 (2014).
26. S. B. Mathew, A. K. Pillai, and V. K. Gupta, *J. Dispers. Sci. Technol.*, **30**, 609 (2009).
27. R. D. Nagarajan, A. Sundaramurthy, and A. K. Sundramoorthy, *Chemosphere*, **286**, 131478 (2022).
28. K. S. Prasad, G. Muthuraman, and J.-M. Zen, *Electrochem. Commun.*, **10**, 559 (2008).
29. B. Uslu and S. A. Ozkan, *Anal. Lett.*, **40**, 817 (2007).
30. R. D. Nagarajan, P. Murugan, K. Palaniyandi, R. Atchudan, and A. K. Sundramoorthy, *Micromachines*, **12**, 862 (2021).
31. A. K. Sundramoorthy, O. Sadak, S. Anandhakumar, and S. Gunasekaran, *J. Electrochem. Soc.*, **163**, B638 (2016).

32. Y. Liang, W. Zhang, D. Wu, Q. Ni, and M. Q. Zhang, *Adv. Mater. Interfaces*, **5**, 1800430 (2018).
33. S. Kubendhiran, S. Sakthinathan, S.-M. Chen, C. M. Lee, B.-S. Lou, P. Sireesha, and C. Su, *Int. J. Electrochem. Sci.*, **11**, 7934 (2016).
34. D. Pan, S. Rong, G. Zhang, Y. Zhang, Q. Zhou, F. Liu, M. Li, D. Chang, and H. Pan, *Electrochemistry*, **83**, 725 (2015).
35. C. Martin and C. Grgicak, *ECS Trans.*, **61**, 1 (2014).
36. R. Gusmão, V. López-Puente, I. Pastoriza-Santos, J. Pérez-Juste, M. F. Proença, F. Bento, D. Geraldo, M. C. Paiva, and E. González-Romero, *RSC Adv.*, **5**, 5024 (2015).
37. Y. Su, C. Tai, and J. Zen, *Electroanalysis*, **25**, 2539 (2013).
38. S. C. Wang, K. S. Chang, and C.-J. Yuan, *Electrochim. Acta*, **54**, 4937 (2009).
39. L. R. Cumba et al., *Analyst*, **141**, 2791 (2016).
40. G. D. Pierini, C. W. Foster, S. J. Rowley-Neale, H. Fernández, and C. E. Banks, *Analyst*, **143**, 3360 (2018).
41. J. Wang, M. Pedrero, H. Sakslund, O. Hammerich, and J. Pingarron, *Analyst*, **121**, 345 (1996).
42. G. Cui, J. H. Yoo, J. S. Lee, J. Yoo, J. H. Uhm, G. S. Cha, and H. Nam, *Analyst*, **126**, 1399 (2001).
43. P. Trogadas, T. F. Fuller, and P. Strasser, *Carbon*, **75**, 5 (2014).
44. Y. Yi, G. Weinberg, M. Prenzel, M. Greiner, S. Heumann, S. Becker, and R. Schlögl, *Catal. Today*, **295**, 32 (2017).
45. D. M. Anjo, M. Kahr, M. M. Khodabakhsh, S. Nowinski, and M. Wanger, *Anal. Chem.*, **61**, 2603 (1989).
46. M. Morita, R. Arizono, N. Yoshimoto, and M. Egashira, *J. Appl. Electrochem.*, **44**, 447 (2014).
47. R. L. McCreery, *Electroanalytical chemistry* (CRC Press, Boca Raton, FL)221 (1991).
48. K. S. Prasad, J.-C. Chen, C. Ay, and J.-M. Zen, *Sensors Actuators B Chem.*, **123**, 715 (2007).
49. M. I. González-Sánchez, B. Gómez-Monedero, J. Agrisuelas, J. Iniesta, and E. Valero, *J. Electroanal. Chem.*, **839**, 75 (2019).
50. A. Dekanski, J. Stevanović, R. Stevanović, B. Ž. Nikolić, and V. M. Jovanović, *Carbon N. Y.*, **39**, 1195 (2001).
51. Y. Teng, T. Chen, F. Xu, W. Zhao, and W. Liu, *Int. J. Electrochem. Sci.*, **11**, 1907 (2016).
52. A. K. Sundramoorthy, S. Mesgari, J. Wang, R. Kumar, M. A. Sk, S. H. Yeap, Q. Zhang, S. K. Sze, K. H. Lim, and M. B. Chan-Park, *J. Am. Chem. Soc.*, **135**, 5569 (2013).
53. A. K. Sundramoorthy, Y. Wang, J. Wang, J. Che, Y. X. Thong, A. C. W. Lu, and M. B. Chan-Park, *Sci Rep.*, **5**, 1 (2015).
54. C. H. A. Wong, A. Ambrosi, and M. Pumera, *Nanoscale*, **4**, 4972 (2012).
55. A. B. Dongil, B. Bachiller-Baeza, A. Guerrero-Ruiz, I. Rodríguez-Ramos, A. Martínez-Alonso, and J. M. D. Tascón, *J. Colloid Interface Sci.*, **355**, 179 (2011).
56. G. Ibáñez-Redín, D. Wilson, D. Gonçalves, and O. N. Oliveira Jr, *J. Colloid Interface Sci.*, **515**, 101 (2018).
57. S. Do Hong, M. Y. Ha, and S. Balachandar, *J. Colloid Interface Sci.*, **339**, 187 (2009).
58. A. Y. Rychagov and Y. M. Volfkovich, *Russ. J. Electrochem.*, **43**, 1273 (2007).
59. S. A. Kumar, H. Cheng, and S. Chen, *Electroanalysis*, **21**, 2281 (2009).
60. P. Murugan, J. Annamalai, R. Atchudan, M. Govindasamy, D. Nallaswamy, D. Ganapathy, A. Reshetilov, and A. K. Sundramoorthy, *Micromachines*, **13**, 304 (2022).
61. S. Teepoo, P. Dawan, and N. Barnthip, *Biosens*, **7**, 47 (2017).
62. D. A. Centeno, X. H. Solano, and J. J. Castillo, *Bioelectrochemistry*, **116**, 33 (2017).
63. L. A. Guerrero, L. Fernández, G. González, M. Montero-Jiménez, R. Uribe, A. Díaz, Barrios, and P. J. Espinoza-Montero, *Nanomater.*, **10**, 64 (2020).
64. J. Wan, W. Wang, G. Yin, and X. Ma, *J. Clust. Sci.*, **23**, 1061 (2012).
65. S. A. Hira, M. Nallal, K. Rajendran, S. Song, S. Park, J.-M. Lee, S. H. Joo, and K. H. Park, *Anal. Chim. Acta*, **1118**, 26 (2020).
66. D. Li, L. Luo, Z. Pang, X. Chen, Y. Cai, and Q. Wei, *RSC Adv.*, **4**, 3857 (2014).